Spectroscopy of $2s_{1/2}-2p_{3/2}$ transitions in W^{65+} through W^{71+}

Y. Podpaly,* J. Clementson, P. Beiersdorfer, J. Williamson,† G. V. Brown, and M. F. Gu
Physics Division, Lawrence Livermore National Laboratory, Livermore, California 94550, USA
(Received 28 August 2009; published 11 November 2009)

A high-resolution flat-crystal spectrometer was used on the SuperEBIT electron beam ion trap to measure the energies of the $2s_{1/2}-2p_{3/2}$ transitions in lithiumlike through fluorinelike tungsten. These transitions are strongly affected by energy shifts due to quantum electrodynamics (QED). SuperEBIT was run at an electron energy of 103.2 ± 0.5 keV and an electron beam current of 150 mA to generate the respective charge states; hydrogenlike aluminum and neonlike krypton were used as calibration elements. The spectra were analyzed with and the results compared to calculations based on the flexible atomic code. Good agreement was found. The measurements yielded line positions with a precision of 1–2 eV, which test QED calculations to 5%–10%.

DOI: 10.1103/PhysRevA.80.052504 PACS number(s): 32.30.Rj, 52.70.La

I. INTRODUCTION

Spectral studies of ions of heavy elements provide data that are invaluable in a variety of fields including atomic physics, astronomy, and high-temperature plasma diagnostics. In atomic physics, transition energies provide a test of the predictions of quantum electrodynamics (QED) as well as a handle on the nature of multielectron atomic structure. The QED contribution to the $2s_{1/2}-2p_{3/2}$ transition has been measured for high-Z elements such as thorium, uranium, and, more recently, lead [1–4] and for mid-Z elements such as xenon [5]; additional experiments are being planned as well such as those on the GSI storage ring [6]. QED processes are generally more pronounced with higher charge, since the effects scale as Z^4. However, QED plays a large role in determining the transition energies of all of these heavy ions. The present work, which focuses on the $2s_{1/2}-2p_{3/2}$ transitions in highly charged tungsten ions, proceeds to fill uncharted territory in mid-to-high-Z elements, i.e., the region in atomic number between Xe ($Z=54$) and Pb ($Z=82$) for which no measurements exist.

Measurements of tungsten have recently become significantly more important due to the start of construction of the ITER tokamak, where tungsten plasma-facing components and high electron temperatures, on the order of 25 keV, possibly reaching as high as 30–40 keV under certain operating conditions [7,8], are expected to produce highly ionized tungsten within the plasma. In fact, line radiation of L-shell tungsten ions may serve as a diagnostic of the ion temperature and the bulk velocity of the plasma core, where such highly charged ions are predicted to exist. Moreover, plasma energy losses can become significant due to radiation, so there has been research on the intensities and energies of the tungsten emissions, mostly in the euv and vuv, covering charge states from W^{64+} and below [9–16]. These investigations have been important both for tokamak and Z pinch plasmas [17,18]. None of these works, however, have focused on QED effects. An exception is the recent measurement of 3–3 transitions in sodiumlike tungsten and neighboring ions with lower charge (W^{58+}-W^{61+}). These measurements achieved an accuracy sufficient to constrain QED calculations at the 10% level [19].

The overall objective of the work described in this paper is to measure with high resolution the $2s_{1/2}-2p_{3/2}$ transitions of highly ionized tungsten L-shell ions, identify the spectral lines, and compare the measured energies to theoretical values. We find that these transitions are the strongest lines in the x-ray spectrum of open L-shell tungsten ions. The QED contribution is expected to be about 17 eV for the $2s_{1/2}-2p_{3/2}$ transition of Li-like tungsten [20]; since our measurement has an accuracy of about 1 eV, it provides a gauge of the QED contribution at the 6% level.

II. EXPERIMENTAL SETUP

The SuperEBIT electron beam ion trap at the Lawrence Livermore National Laboratory (LLNL) [21] was used to make these measurements in a Doppler-shift free, tungsten dominated environment. An electron beam ion trap employs a set of drift tubes and uses the space charge effect of the electron beam to create an electrostatic potential trap to confine the ions to be studied. A 3 T axial magnetic field is used to further confine the ions. Due to the possible buildup of impurities in the trap, the axial well is emptied at a given frequency to purge all confined ions. For these measurements the electron beam energy was set to 103.2 ± 0.5 keV and the timing cycle was chosen to produce the best tungsten charge balance, which was found to be 27 s. Beam currents were maintained around approximately 150 mA. Tungsten was injected into the trap with a metal vapor vacuum arc. There were trace amounts of argon and silicon in the trap; these elements acted as low-Z cooling ions and provided x-ray calibration lines. At these machine parameters, the 2–2 transitions of tungsten are the most significant emission seen, as illustrated in the spectrum recorded with the EBIT x-ray calorimeter spectrometer (ECS) in Fig. 1. The ECS [22,23] has an energy resolution of approximately 5 eV across the energy range 0.5–15 keV. It does not have the resolution of a crystal spectrometer, but it is an exceptional survey diagnostic.

*Permanent address: MIT Plasma Science and Fusion Center, Cambridge, MA 02139.
†Department of Physics, Florida A&M University, Tallahassee, FL 32307.

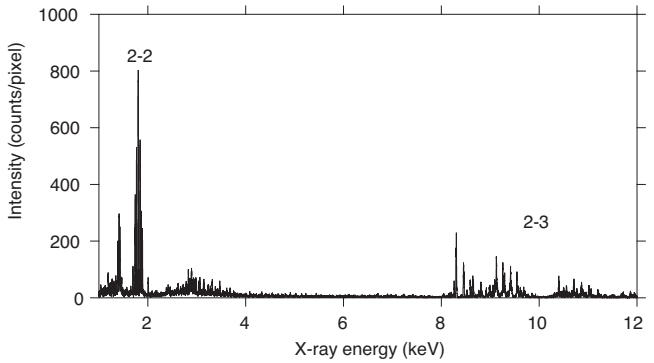

FIG. 1. Spectrum of tungsten from SuperEBIT recorded with the EBIT calorimeter spectrometer (ECS). Transitions between levels of principal quantum number n are labeled.

The crystal spectrometer we employed for the present measurement used a 11-cm-long, 1.2-cm-wide flat ammonium dihydrogen phosphate (ADP, $2d=10.640$ Å) crystal 38 cm from the electron beam and set to a central Bragg angle of $\theta=39°$. X rays were detected with an ORDELA model 1100XF position-sensitive proportional counter placed at a distance of 25 cm from the crystal. The detector was filled with 760 Torr P-10 gas (90% argon, 10% methane). The detector's vacuum window consisted of 4 μm polyimide coated with 200–400 Å aluminum. Further descriptions of the spectrometer are available in [24,25]. The crystal reflects x rays based on their wavelengths, λ, following Bragg's law, $n\lambda=2d\sin(\theta)$, where n is the order of reflection. The position on the detector, thus, can give precise wavelength information. The spectrometer was operated with a chamber pressure on the order of 10^{-7} Torr, which is a factor of 10^4 higher than the ambient EBIT chamber pressure. This pressure gradient is maintained using a 5076 Å thick polyimide filter. The detector is connected to an event-mode-type data acquisition system [26].

The spectrometer was calibrated initially with a 1.69 mCi ^{55}Fe source, which allowed setting the gates of the data acquisition system to remove background noise; the ^{55}Fe source was also used to set the proper detector voltage. Spectral lines from hydrogenlike aluminum and neonlike krypton generated in SuperEBIT were used to get a calibration of the energy scale as detailed in the next section. Due to possible drifts in the spectrometer, data from each day were analyzed separately and errors were increased to account for possible drifts.

III. CALIBRATION

The energy calibration of the crystal spectrometer was accomplished by the injection of tri-methyl aluminum (TMA) and krypton gas into the trap. The results of the aluminum calibration are shown in Fig. 2. The spectrum also shows lines from silicion, an intrinsic impurity. The intensity of the silicon emission was too low for both the He-like w and z lines, corresponding to the transitions $1s_{1/2}2p_{3/2}\rightarrow 1s^2$ and $1s_{1/2}2s_{1/2}\rightarrow 1s^2$, respectively, to provide an accurate calibration; however, the w line was located where it was expected. Neonlike krypton has the four strong, well known lines $3F$, $3D$, $3C$, and $3A$ within the region of interest. These lines correspond to the transitions from the upper configurations $2s^22p_{1/2}2p_{3/2}^4 3s_{1/2}$, $2s^22p_{1/2}^2 2p_{3/2}^3 3d_{5/2}$, $2s^22p_{1/2}2p_{3/2}^4 3d_{3/2}$, and $2s_{1/2}2p^6 3p_{3/2}$, respectively, to the ground state $2s^22p^6$. There are numerous other krypton lines in the region as well, mostly from fluorinelike krypton; however, these lines were overly blended to use for calibration. The krypton measurement is shown in Fig. 3. Since each x-ray energy is directly related via Bragg's law to a unique angle on the detector face, the calibration curve was calculated as a relation between angle and channel number.

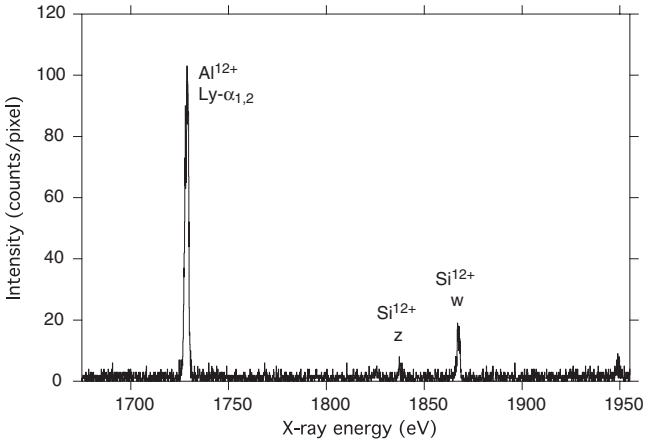

FIG. 2. Spectrum of hydrogenlike aluminum recorded on SuperEBIT with the flat-crystal spectrometer. Additional lines from heliumlike silicon are marked as well. These lines are used for wavelength calibrations.

Due to the geometry of the flat crystal and detector arrangement, the curve of angle versus channel number is expected to be a weak quadratic polynomial. The energies of the aluminum lines were set to the values given in [27]. The spectral fitting procedures assumed that the widths of the two Lyman alpha lines were identical, since the linewidth in our case was almost exclusively determined by the detector res-

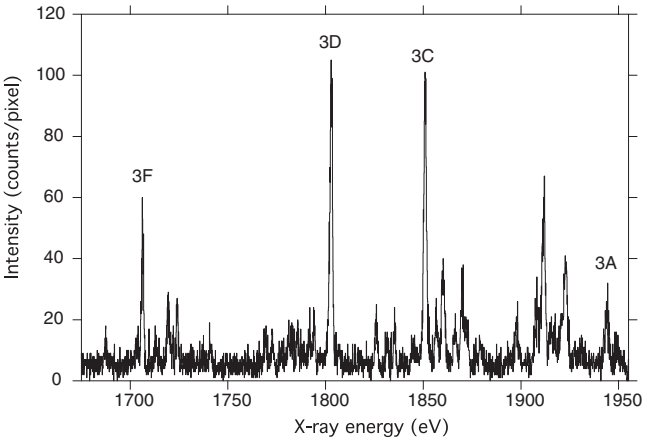

FIG. 3. Spectrum of neonlike krypton recorded on SuperEBIT with the flat-crystal spectrometer. Unlabeled lines are mostly from fluorinelike krypton. The neonlike krypton lines are used for wavelength calibrations.

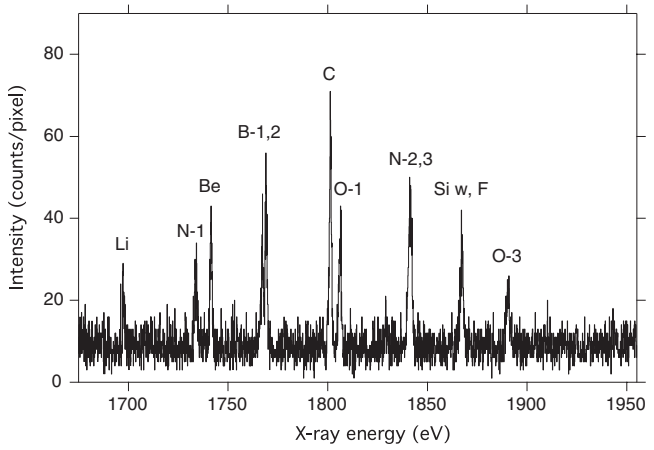

FIG. 4. Spectrum of the $2_{1/2}-2p_{3/2}$ transitions of tungsten recorded on SuperEBIT with the flat-crystal spectrometer. The lines are labeled using the isoelectronic notation from Table I.

olution. The krypton line energies were taken from [28]; and we again fitted them with equal widths. To test this, all lines were also fit individually, but none of the fits suggested an asymmetric detector response, and all lines had equal widths unless they were blended with other lines. The statistical errors for the line centroids in channel number and the published uncertainties for the energies of the krypton and aluminum calibration lines yielded an error box, the area of which was taken as the inverse weight of the point. Due to the large error bars on the krypton reference lines, the highest justifiable order of the fitting polynomial was 1 (linear). The calibration curve was found to be

$$\lambda = 10.640 \sin(45.76 \pm 0.03 - C \times 0.003\,227 \pm 1.836 \times 10^{-5}), \quad (1)$$

where C is the detector channel number and the units are angstroms.

IV. RESULTS AND ANALYSIS

Tungsten data from five run days were analyzed. No noticeable drift in the line and, thus, spectrometer position was found. The spectra were, therefore, summed; the resulting spectrum is shown in Fig. 4. Line positions, however, were obtained by taking each individual day's data, assuming equal widths, and finding the average centroid by weighting the results by the number of counts in the line of each day. Using the flexible atomic code (FAC) [29] and published references, the transitions giving rise to these peaks were identified. FAC is a self-contained fully relativistic code capable of calculating various atomic characteristics such as atomic levels, autoionization, and electron impact excitation. FAC calculates the atomic levels, which were used in this paper, by solving the Dirac-Coulomb Hamiltonian and including QED effects such as retardation and recoil; vacuum polarization and self-energy effects are implemented using a screened hydrogenic approximation.

Unfortunately, the intrinsic silicon impurities in the trap blended with two nitrogenlike tungsten peaks near 1840 eV and the fluorinelike tungsten peak. The fluorinelike tungsten peak was only resolvable for one of the run days, when the silicon admixture to the plasma was negligible. Hence, that value was taken and has been listed in Table I. From the calibration data, it was seen that the contribution from line z of He-like silicon to the nitrogenlike peaks was around 25 counts per day, which ended up being approximately 17% of the total line area. Due to the presence of two nitrogenlike peaks and uncertainties in the actual number of silicon w counts, deconvolution was not possible and the error bars on the nitrogenlike transitions had to be widened to account not only for their overlap but also for the blend with the silicon peak. Further uncertainties were approximated by analyzing the individual run days' data for deviations from a perfect Gaussian line profile.

The lithiumlike line was situated outside of the calibrated interval. The uncertainty in the inferred energy of this line

TABLE I. Summary of measured tungsten lines and comparison with theoretical values. Errors and theoretical source are shown. All energies are in eV, intensities in arbitrary units, and Einstein coefficients in s^{-1}.

Measured value	Theoretical[a]	Amplitude	A_{ij} (units of 10^{13})	Transition	Stage
1697.34 ± 1.03	1695.9956[b],1697.6	16.904 ± 1.63	0.7988	$(1s^2 2s_{1/2})_{J=1/2}-(1s^2 2p_{3/2})_{J=3/2}$	Li
1733.55 ± 1.20	1735.5	24.444 ± 1.64	0.294	$(1s^2 2s^2 2p_{1/2}^2 2p_{3/2})_{J=3/2}-(1s^2 2s_{1/2} 2p_{1/2}^2 2p_{3/2}^2)_{J=5/2}$	N-1
1741.08 ± 1.25	1743.8	30.824 ± 1.66	1.156	$(1s^2 2s^2)_{J=0}-(1s^2 2s_{1/2} 2p_{3/2})_{J=1}$	Be
1766.62 ± 1.39	1769.4	25.946 ± 1.72	1.283	$(1s^2 2s^2 2p_{1/2})_{J=1/2}-(1s^2 2s_{1/2} 2p_{1/2} 2p_{3/2})_{J=1/2}$	B-2
1768.71 ± 1.40	1771.2	37.127 ± 1.74	1.173	$(1s^2 2s^2 2p_{1/2})_{J=1/2}-(1s^2 2s_{1/2} 2p_{1/2} 2p_{3/2})_{J=3/2}$	B-1
1801.07 ± 1.60	1803.9	48.787 ± 1.72	1.266	$(1s^2 2s^2 2p_{1/2}^2)_{J=0}-(1s^2 2s_{1/2} 2p_{1/2}^2 2p_{3/2})_{J=1}$	C
1805.91 ± 1.63	1808.4	29.777 ± 1.66	1.020	$(1s^2 2s^2 2p_{1/2}^2 2p_{3/2}^2)_{J=2}-(1s^2 2s_{1/2} 2p_{1/2}^2 2p_{3/2}^3)_{J=2}$	O-1
1840.44 ± 1.90	1842.6	17.977 ± 1.63	1.091	$(1s^2 2s^2 2p_{1/2}^2 2p_{3/2})_{J=3/2}-(1s^2 2s_{1/2} 2p_{1/2}^2 2p_{3/2}^2)_{J=1/2}$	N-2
1841.84 ± 1.88	1844.1	14.614 ± 2.98	2.023	$(1s^2 2s^2 2p_{1/2}^2 2p_{3/2})_{J=3/2}-(1s^2 2s_{1/2} 2p_{1/2}^2 2p_{3/2}^2)_{J=3/2}$	N-3
1871.16 ± 2.10	1869.9	N/A[c]	2.232	$(1s^2 2s^2 2p_{1/2}^2 2p_{3/2}^3)_{J=3/2}-(1s^2 2s_{1/2} 2p_{1/2}^2 2p_{3/2}^4)_{J=1/2}$	F
1891.01 ± 2.25	1893.3	17.977 ± 1.63	1.886	$(1s^2 2s^2 2p_{1/2}^2 2p_{3/2}^2)_{J=2}-(1s^2 2s_{1/2} 2p_{1/2}^2 2p_{3/2}^3)_{J=1}$	O-3

[a]Calculations performed using FAC.
[b]Value from Kim *et al.* [20].
[c]Data were only available from one day, so comparing this count rate to that of the other transitions is not possible.

was increased by the uncertainty given by extrapolating the calibration curve, approximately 0.12 eV.

The data are summarized in Table I along with theoretical predictions and the line identifications. All uncertainties stated refer to one standard deviation; the 95% confidence interval is found by multiplying the given errors by approximately 1.96.

The observed tungsten lines were identified based on several criteria. First, since the SuperEBIT trap is filled with a low-density plasma, most observed lines are from transitions connecting to the ground state. Second, the most likely transitions are selected based on the FAC calculated transition energies and transition probabilities. Furthermore, extensive studies, both experimental and theoretical, of the line intensities have been made for uranium and thorium [1,30], and the strong lines expected in tungsten are presumed to not differ much from those in thorium and uranium, although their relative positions may move and are, in fact, seen to interchange. The previous research on thorium suggests the existence of a third oxygenlike line within this transition band at approximately 20% the intensity of the strong line. Calculations place that line around 1832 eV with an Einstein coefficient of 6.5×10^{12} s^{-1}; this line cannot be resolved from the background with sufficient certainty; however, it does appear to exist visually at the predicted location.

The tungsten line intensities were obtained by analyzing the heights above background as found from the summed data. Comparing the measured relative line intensities within an ionization stage with the Einstein coefficients as calculated by FAC show good agreement, which indicates that direct electron-impact excitation is the dominant line formation mechanism for these dipole-allowed transitions. The two nitrogenlike lines near 1840 eV, unfortunately, are blended, so their relative intensity measurements are not certain. The fluorinelike line intensity was only seen in one run day, so its intensity could not be extrapolated to the full run period. The constants that were used here in order to convert wavelength and energy are $h=6.626\ 068\ 96\times10^{-34}$ J s, $c=2.997\ 924\ 58\times10^{8}$ m/s, and $e=1.602\ 176\ 487\times10^{-19}$ C.

V. SUMMARY AND DISCUSSION

The line positions of the resonance lines in lithiumlike through fluorinelike tungsten have been measured. This work has extended the lithiumlike isoelectronic sequence, which has only a single valence electron, into the region of atomic number between xenon ($Z=54$) and lead ($Z=82$), where no data were available. The $2s_{1/2}-2p_{3/2}$ line position is affected by a QED contribution of about 17 eV. Our measurements are sensitive to 6% of this effect. Providing data in this range of atomic number is even more important for the berylliumlike to fluorinelike charge states of tungsten. For these ionic states no highly accurate theoretical calculations are yet available and electron-electron correlations strongly affect the energy levels, as discussed in a recent review by Cheng *et al.* [31]

The knowledge of the energies of the tungsten $2s_{1/2}-2p_{3/2}$ lines is very important for diagnostics of hot plasmas. As our line survey has shown in Fig. 1, these are the brightest x-ray lines from open *L*-shell tungsten ions. These lines appear at high electron temperatures, and similarly high ion temperatures in a thermal plasma significantly broaden the lines. At 30–40 keV ion temperature, which is not unrealistic in the ITER tokamak, the linewidths will be approximately 2 eV. Because different charge states exist in different albeit neighboring locations in the plasma, measurement of the $2s_{1/2}-2p_{3/2}$ spectrum of tungsten can yield temperature values at different locations in the plasma. Furthermore, the shift in the position of the line is a diagnostic for plasma rotation [32]. The data presented in this paper can serve as a basis for using these lines as a diagnostic tool.

ACKNOWLEDGMENTS

The authors would like to recognize D. Thorn, M. Frankel, E. Magee, and E. Träbert for their technical support and advice. Y.P. would also like to thank J. E. Rice for his support and comments. This work was performed at Lawrence Livermore National Laboratory under the auspices of the Department of Energy under Contract No. DE-AC52-07NA-27344 and was supported by the Laboratory Directed Research and Development program under Project No. 09-ERD-013. Y.P. acknowledges support from the Fusion Energy Sciences Program, administered by Oak Ridge Institute of Science and Education under a contract between the U.S. Department of Energy and the Oak Ridge Associated Universities. J. W. acknowledges support by NSF Grant HRD-0630370.

[1] P. Beiersdorfer, D. Knapp, R. E. Marrs, S. R. Elliott, and M. H. Chen, Phys. Rev. Lett. **71**, 3939 (1993).
[2] P. Beiersdorfer, A. L. Osterheld, and S. R. Elliott, Phys. Rev. A **58**, 1944 (1998).
[3] X. Zhang, N. Nakamura, C. Chen, M. Andersson, Y. Liu, and S. Ohtani, Phys. Rev. A **78**, 032504 (2008).
[4] P. Beiersdorfer, S. R. Elliott, A. L. Osterheld, T. Stöhlker, J. Autrey, G. V. Brown, A. J. Smith, and K. Widmann, Phys. Rev. A **53**, 4000 (1996).
[5] T. Mooney, E. Lindroth, P. Indelicato, E. G. Kessler, and R. D. Deslattes, Phys. Rev. A **45**, 1531 (1992).
[6] M. Trassinelli, D. Banaś, H. F. Beyer, P. Jagodz'nski, A. Kumar, M. Pajek, and T. Stöhlker, Can. J. Phys. **85**, 441 (2007).
[7] C. Gormezano *et al.*, Nucl. Fusion **47**, S285 (2007).
[8] A. J. H. Donné *et al.*, Nucl. Fusion **47**, S337 (2007).
[9] R. Neu, K. B. Fournier, D. Schlögl, and J. Rice, J. Phys. B **30**, 5057 (1997).
[10] Y. Ralchenko, I. N. Draganic, J. N. Tan, J. D. Gillaspy, J. M. Pomeroy, J. Reader, U. Feldman, and G. E. Holland, J. Phys. B **41**, 021003 (2008).
[11] T. Pütterich, R. Neu, C. Biedermann, R. Radtke, and the ASDEX Upgrade Team, J. Phys. B **38**, 3071 (2005).

[12] C. Biedermann, R. Radtke, J.-L. Schwob, P. Mandelbaum, R. Doron, T. Fuchs, and G. Fußmann, Phys. Scr. **T92**, 85 (2001).
[13] P. Neill, C. Harris, A. S. Safranova, S. Hamasha, S. Hansen, U. I. Safronova, and P. Beiersdorfer, Can. J. Phys. **82**, 931 (2004).
[14] S. B. Utter, P. Beiersdorfer, and E. Träbert, Can. J. Phys. **80**, 1503 (2002).
[15] C. H. Skinner, Can. J. Phys. **86**, 285 (2008).
[16] J. Clementson, P. Beiersdorfer, G. V. Brown, and M. F. Gu (unpublished).
[17] A. S. Safronova *et al.*, Can. J. Phys. **86**, 267 (2008).
[18] N. J. Peacock, M. G. O'Mullane, R. Barnsley, and M. Tarbutt, Can. J. Phys. **86**, 277 (2008).
[19] J. D. Gillaspy, I. N. Draganic, Y. Ralchenko, J. Reader, J. N. Tan, J. M. Pomeroy, and S. M. Brewer, Phys. Rev. A **80**, 010501(R) (2009).
[20] Y.-K. Kim, D. H. Baik, P. Indelicato, and J. P. Desclaux, Phys. Rev. A **44**, 148 (1991).
[21] D. A. Knapp, R. E. Marrs, S. R. Elliott, E. W. Magee, and R. Zasadzinski, Nucl. Instrum. Methods Phys. Res. A **334**, 305 (1993).
[22] F. S. Porter *et al.*, J. Low Temp. Phys. **151**, 1061 (2008).
[23] F. S. Porter *et al.*, Can. J. Phys. **86**, 231 (2008).
[24] G. V. Brown, P. Beiersdorfer, and K. Widmann, Rev. Sci. Instrum. **70**, 280 (1999).
[25] P. Beiersdorfer, G. V. Brown, R. Goddard, and B. J. Wargelin, Rev. Sci. Instrum. **75**, 3720 (2004).
[26] P. Beiersdorfer, G. V. Brown, L. Hildebrandt, K. L. Wong, and R. Ali, Rev. Sci. Instrum. **72**, 508 (2001).
[27] W. R. Johnson and G. Soff, At. Data Nucl. Data Tables **33**, 405 (1985).
[28] J. E. Rice, K. B. Fournier, J. A. Goetz, E. S. Marmar, and J. L. Terry, J. Phys. B **33**, 5435 (2000).
[29] M. F. Gu, Can. J. Phys. **86**, 675 (2008).
[30] P. Beiersdorfer, A. Osterheld, S. R. Elliott, M. H. Chen, D. Knapp, and K. Reed, Phys. Rev. A **52**, 2693 (1995).
[31] K. T. Cheng, M. H. Chen, W. R. Johnson, and J. Sapirstein, Can. J. Phys. **86**, 33 (2008).
[32] M. Bitter, G. Bertschinger, W. Biel, R. Jaspers, I. Ahmad, J. Weinheimer, and H.-J. Kunze, *27th Conference on Controlled Fusion and Plasma Physics, 2000*, Europhysics Conference Abstracts Vol. 24B, p. 840 (2000).